A unit cell wave based reduced order modelling approach for fast vibration response calculations of finite periodic metamaterial plates

F. Qu [1,3,4], **L. Van Belle** [1,3], **E. Deckers** [2,3]
[1] KU Leuven, Department of Mechanical Engineering,
Celestijnenlaan 300, B-3001, Heverlee, Belgium
e-mail: **fei.qu@kuleuven.be**

[2] KU Leuven, Campus Diepenbeek, Department of Mechanical Engineering,
Wetenschapspark 27, B-3590 Diepenbeek, Belgium

[3] DMMS Core lab, Flanders Make, Belgium

[4] SIM M3 program,
Technologiepark 48, B-9052 Zwijnaarde, Belgium

Abstract
In the past decades, periodic structures and metamaterials in particular have attracted significant attention as innovative noise and vibration control solutions which can combine lightweight requirements with favourable vibro-acoustic performance. To predict their vibro-acoustic performance, periodicity is generally exploited by considering a single finite element unit cell model and calculating dispersion curves. However, to predict their vibration attenuation performance in real-life applications, finite structures are of interest. Due to the often complex and detailed nature of the unit cells, the unit cell finite element models can become large, which would rapidly render finite structure models comprised of unit cell assemblies computationally unaffordable. To overcome this problem, in this work, a wave based reduced order modelling approach is proposed to efficiently compute forced vibration responses of planar finite periodic plates.

1 Introduction

Architected structures with stop band behaviour, such as phonic crystals (PCs) and locally resonant metamaterials (LRMs), open the door towards novel lightweight vibroacoustic solutions, attenuating incoming noise and vibration in a targeted frequency range [1, 2]. These structures are mostly represented by a periodic repetition of unit cells (UCs). To predict the stop band, the so-called UC modelling approach is used, where an infinite periodic structure is often assumed so that the Bloch-Floquet (BF) periodic boundary conditions (BCs)can be applied to a single UC model and the band structure is calculated by solving the resulting dispersion eigenvalue problem (EVP) [3]. The UC model is often built using the finite element method (FEM) as it allows high geometrical complexity [4, 5]. However, the intricate geometries or material distribution of the UCs can result in large sized UC models and the band structure calculations can become computationally expensive. Therefore, several reduced order modelling approaches have been introduced, such as the Bloch mode synthesis (BMS) [6], the generalized Bloch mode synthesis (GBMS) [7] and the reduced Bloch mode expansion (RBME) [8] to speed up dispersion band structure computations. In practice, however, the predicted stop band by assuming infinite periodicity may not be preserved in its finite counterpart due to the effect of the BCs [9]. This strongly limits the use of UC models for real-life applications.

To be able to compute the forced vibration response of finite periodic structures, assemblies of many UCs have to be dealt with. Such full-scale FE models would require higher computational effort. To reduce

the computation time and memory, various methods for model order reduction (MOR) of finite periodic structures have recently been developed and can be catagorized into two types: substructuring and wave expansion methods [10]. The former follows the rationale of the Craig-Bampton method, where a single UC is firstly partitioned with interior and interface degrees of freedom (DOFs) and reduced through the projection based approaches. Next, the full system is constructed by assembling the identical reduced UC models, after which the frequency or time domain reduction method is applied to the assembled full system to further accelerate the vibration response calculations. Several combinations of UC and full structure reduction approaches are developed: van Ophem et al. applied Krylov subspace to reduce the UC model and applied the Automatic Krylov Subspace Algorithm (ASKA) for the full system [11], Mencik et al. uses the BMS to build the basis for interior DOFs of the UC model [12], Van Belle et al. improves the efficiency of the UC reduction by applying the GBMS which allows to further reduce the UC interface DOFs resulting in a smaller UC reduced order model (ROM) and reduces the assembled full system using the eigen modes and the static enrichment as global basis [13]. Although the computational effort is significantly reduced, the step of building the global basis can still be expensive since the encountered full system scales linearly with the number of UCs. On the other hand, the MOR methods based on the wave expansion [14, 15] enable higher reduction as they build the global basis only on the local UC model: the global basis is built through the free or forced vibration waves of the corresponding infinite periodic structure. Thanks to the infinite periodicity, the Bloch waves can be solved cheaply using the UC modelling approach without dealing with the full system. However, the current wave expansion based approaches are limited to 1D periodic structures, which cannot take the full advantage of the periodicity when 2D and 3D periodic structures are encountered.

To further improve the efficiency by fully utilizing the periodicity, a reduced order modelling approach is introduced following the rationale of the wave based method (WBM) [16]. This method belongs to the family of indirect Trefftz methods. It approximates the dynamic field variables using a weighted sum of wave functions which are exact solution of the governing partial differential equations (PDEs). By minimising the errors on BCs in a weighted residual sense, a system of equations is obtained and solved for the unknown contribution factors of each wave function. However, unlike the typical WBM which starts from exact analytical solutions to the governing PDEs in simplified domains, the analytical wave functions are not available for structures composed of arbitrary UC assemblies. To overcome this, in this work, the use of the UC modelling approach is proposed to calculate the wave functions by solving a dispersion EVP for a single UC FE model.

The rest of this paper is organized as follows: In Section 2, the problem description is presented. Section 3 details the reduced order modelling approach for periodic structures based on the idea of the WBM. In Section 4, a convergence study is presented with respect to the input parameters of the approach and the accuracy and computation time are compared to the dynamic substructuring approach for an increasing number of UCs are performed. Finally, the main conclusions are summarized in Section 5.

2 Problem description

In this work, rectangular metamaterial plates are considered, which are composed of a 2D repetition of a single UC in a rectangular periodic grid as shown in Fig.1. The plate is subjected to a given external load $\mathbf{f}$ inside the domain Ω, the traction $\mathbf{T}$ and the displacement constraints on the boundary Γ. In this model, the material and kinematic linearity are assumed and a steady state response is considered. Therefore, the model is analysed for the vibration response in the frequency domain.

3 Methodology

In this section, the general rationale and overview of the approach are first introduced in Section 3.1. After that, each building block of the approach is illustrated: the UC FE model and the UC reduction in Section 3.2, the overview of the wave finite element method (WFEM) in Section 3.3, the calculation of free and forced vibration waves in Section 3.4 and Section 3.5, the evaluation of UC waves on the boundary of the finite structure and the calculation of the contribution factors as well as the back projection in Section 3.6.

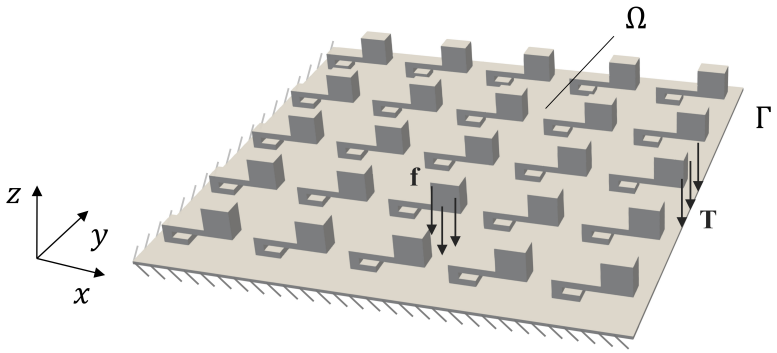

Figure 1: Schematic of a periodic metamaterial plate composed of 5×5 UCs.

3.1 General rationale and overview of the approach

Following the WBM, the displacement field $\mathbf{u}$ of the finite plate is approximated using a linear superposition of free and forced vibration waves [16]:

$$\mathbf{u}(x, y, z) \approx \hat{\mathbf{u}} = \sum_{\alpha=1}^{N} \mathrm{c}_\alpha \mathbf{\Phi}_\alpha + \mathbf{\Phi}_p, \tag{1}$$

where N is the number of free vibration waves taken into account, c_α are unknown contribution factors of each free vibration wave $\mathbf{\Phi}_\alpha$, which satisfies the equilibrium equation of the corresponding free infinite structure at a given frequency. $\mathbf{\Phi}_p$ is a forced vibration wave which is also the particular solution of the corresponding infinite structure for the given external load $\mathbf{f}$ at the same frequency value.

Contrary to the classical WBM, the wave sets of $\mathbf{\Phi}_\alpha$ and $\mathbf{\Phi}_p$ have to be computed numerically since they are not readily available for the arbitrary complex periodic metamaterial plates. As the summation Eq.(1) satisfies the equilibrium equation everywhere inside the domain Ω (Fig.1), the equilibrium condition is only violated on the boundary of the finite plate structure. Therefore, by minimizing the errors on the BCs, the displacement field is solved from a system in the equations of unknown contribution factors c_α. The flow chart (Fig.2) gives the overview of the procedure. The following sections illustrate each of the building blocks of the flow chart in detail.

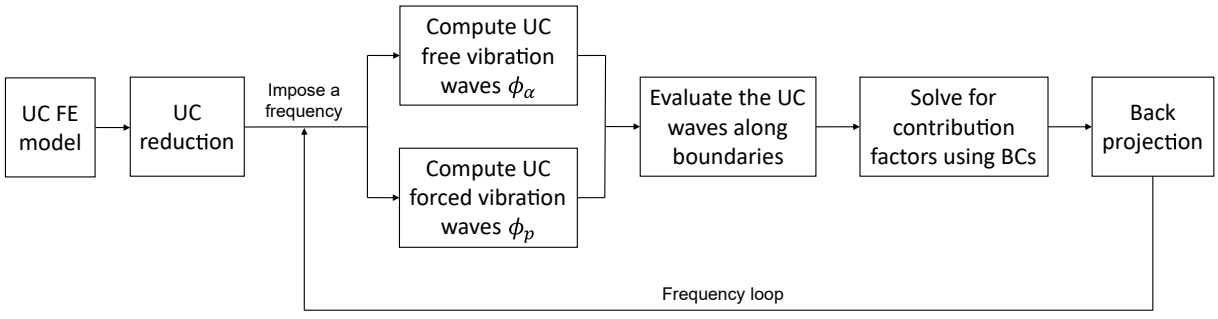

Figure 2: Flow chart of the approach.

3.2 UC FE model and model reduction

The UC is firstly discretized using the FEM (Fig.3). The governing equation of the UC in the frequency domain is written as:

$$\mathbf{D}_{UC}(\omega)\mathbf{U}_{UC} = \mathbf{F}_{UC}, \tag{2}$$

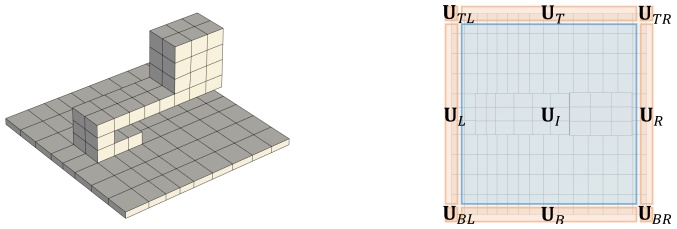

(a) (b)

Figure 3: Example FE discretization of the UC model (a) and top view of the FE UC model partitioned according to interior DOFs (blue) and interface DOFs (orange) (b).

where $\mathbf{D}_{UC} = -\omega^2\mathbf{M}_{UC} + i\omega\mathbf{C}_{UC} + \mathbf{K}_{UC}$ is the dynamic stiffness matrix of the UC. $\mathbf{M}_{UC}$, $\mathbf{C}_{UC}$ and $\mathbf{K}_{UC}$ are the mass, damping, stiffness matrices of the UC, respectively, ω is the given angular frequency of interest, $\mathbf{F}_{UC}$ is the external force on the UC and $i^2 = -1$.

As the UCs FE model is generally of large size due to the complex geometry, UC MOR is applied to enable efficient computation of the wave basis. Here the reduced UC model is computed using the GBMS [7]. First, the interior and interface DOFs are partitioned following Fig.3:

$$\begin{bmatrix} \mathbf{D}_{II} & \mathbf{D}_{IA} \\ \mathbf{D}_{AI} & \mathbf{D}_{AA} \end{bmatrix} \begin{bmatrix} \mathbf{U}_I \\ \mathbf{U}_A \end{bmatrix} = \begin{bmatrix} \mathbf{0} \\ \mathbf{F}_A \end{bmatrix}, \tag{3}$$

where subscripts I and A indicate the interior and the interface DOFs of the UC, respectively, and $\mathbf{U}_A^T = \begin{bmatrix} \mathbf{U}_L^T & \mathbf{U}_B^T & \mathbf{U}_R^T & \mathbf{U}_T^T & \mathbf{U}_{BL}^T & \mathbf{U}_{BR}^T & \mathbf{U}_{TR}^T & \mathbf{U}_{TL}^T \end{bmatrix}$, the force on the interior DOFs $\mathbf{F}_I$ is absent since no external force is imposed.

Then UC DOFs are reduced using a truncated set of interior normal modes and interface modes:

$$\begin{bmatrix} \mathbf{W}_I \\ \mathbf{W}_A \end{bmatrix} = \begin{bmatrix} \mathbf{V}_I & \mathbf{\Psi}_{IA}\mathbf{V}_A \\ \mathbf{0} & \mathbf{V}_A \end{bmatrix} \begin{bmatrix} \mathbf{U}_I \\ \mathbf{U}_A \end{bmatrix}, \tag{4}$$

where $\mathbf{W}_I$ and $\mathbf{W}_A$ are the reduced DOFs of the corresponding UC DOFs of $\mathbf{U}_I$ and $\mathbf{U}_A$, $\mathbf{\Psi}_{IA} = \mathbf{K}_{II}^{-1}\mathbf{K}_{IA}$ is the matrix of static constraint modes, $\mathbf{V}_I$ and $\mathbf{V}_A$ are the matrices of $\mathbf{n}_I$ interior and $\mathbf{n}_A$ interface modes [7].

3.3 Overview of the WFEM

The Floquet propogator imposes a certain way that the UC wave propagates or decays through the infinite periodic structure (Fig.4). When the system vibrates according to one of these waves, the ratio between the displacement field of neighbouring UCs along x or y direction is a constant, which is defined as the propagation constant λ_x or λ_y. However, since the interface displacements between neighboring UCs must be compatible and the interface forces must be balanced, the BF BCs are introduced that every single UC must satisfy (Fig.5). As the UCs are identical to each other, only one UC is considered.

The compatibility condition of the UC displacement is written as:

$$\mathbf{U}_{UC} = \mathbf{\Lambda}_R\mathbf{U}_{UC}^{red} \tag{5}$$

and the force balance at the UC interface is written as:

$$\mathbf{\Lambda}_L\mathbf{P}_{UC} = \mathbf{0} \tag{6}$$

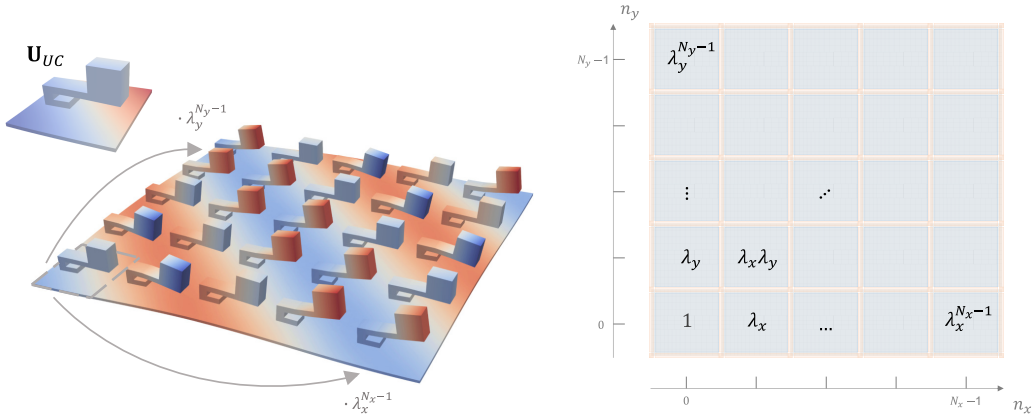

(a) (b)

Figure 4: UC wave propagation (a) and Floquet propogator on the periodic metamaterial plate (b).

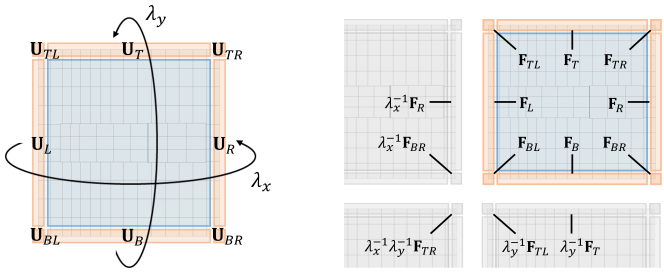

(a) (b)

Figure 5: BF BCs for the single UC: compatibility conditions (a) and equilibrium conditions (b).

where

$$\mathbf{U}_{UC}^T = \begin{bmatrix}\mathbf{U}_I^T & \mathbf{U}_L^T & \mathbf{U}_B^T & \mathbf{U}_R^T & \mathbf{U}_T^T & \mathbf{U}_{BL}^T & \mathbf{U}_{BR}^T & \mathbf{U}_{TR}^T & \mathbf{U}_{TL}^T\end{bmatrix},$$

$$\mathbf{U}_{UC}^{red\,T} = \begin{bmatrix}\mathbf{U}_I^T & \mathbf{U}_L^T & \mathbf{U}_B^T & \mathbf{U}_{BL}^T\end{bmatrix},$$

$$\mathbf{P}_{UC}^T = \begin{bmatrix}\mathbf{P}_I^T & \mathbf{P}_L^T & \mathbf{P}_B^T & \mathbf{P}_R^T & \mathbf{P}_T^T & \mathbf{P}_{BL}^T & \mathbf{P}_{BR}^T & \mathbf{P}_{TR}^T & \mathbf{P}_{TL}^T\end{bmatrix},$$

$$\mathbf{\Lambda}_L = \begin{bmatrix} \mathbf{I} & \mathbf{0} & \mathbf{0} & \mathbf{0} & \mathbf{0} & \mathbf{0} & \mathbf{0} & \mathbf{0} & \mathbf{0} \\ \mathbf{0} & \mathbf{I} & \mathbf{0} & \lambda_x^{-1}\mathbf{I} & \mathbf{0} & \mathbf{0} & \mathbf{0} & \mathbf{0} & \mathbf{0} \\ \mathbf{0} & \mathbf{0} & \mathbf{I} & \mathbf{0} & \lambda_y^{-1}\mathbf{I} & \mathbf{0} & \mathbf{0} & \mathbf{0} & \mathbf{0} \\ \mathbf{0} & \mathbf{0} & \mathbf{0} & \mathbf{0} & \mathbf{0} & \mathbf{I} & \lambda_x^{-1}\mathbf{I} & \lambda_x^{-1}\lambda_y^{-1}\mathbf{I} & \lambda_y^{-1}\mathbf{I} \end{bmatrix},$$

$$\mathbf{\Lambda}_R^T = \begin{bmatrix} \mathbf{I} & \mathbf{0} & \mathbf{0} & \mathbf{0} & \mathbf{0} & \mathbf{0} & \mathbf{0} & \mathbf{0} & \mathbf{0} \\ \mathbf{0} & \mathbf{I} & \mathbf{0} & \lambda_x\mathbf{I} & \mathbf{0} & \mathbf{0} & \mathbf{0} & \mathbf{0} & \mathbf{0} \\ \mathbf{0} & \mathbf{0} & \mathbf{I} & \mathbf{0} & \lambda_y\mathbf{I} & \mathbf{0} & \mathbf{0} & \mathbf{0} & \mathbf{0} \\ \mathbf{0} & \mathbf{0} & \mathbf{0} & \mathbf{0} & \mathbf{0} & \mathbf{I} & \lambda_x\mathbf{I} & \lambda_x\lambda_y\mathbf{I} & \lambda_y\mathbf{I} \end{bmatrix}.$$

Imposing the BF BCs on the governing equation (Eq.(2)) of the UC, the free and forced vibration waves can now be solved from the following equation:

$$\mathbf{\Lambda}_L(\mathbf{D}_{UC}(\omega)\mathbf{\Lambda}_R\mathbf{U}_{UC}^{red} - \mathbf{F}_{UC}) = \mathbf{0}, \tag{7}$$

where the balance of the residual force $\mathbf{P}_{UC} = \mathbf{D}_{UC}\mathbf{\Lambda}_R\mathbf{U}_{UC}^{red} - \mathbf{F}_{UC}$ is satisfied through the Bloch-Floquet BCs (Eq.(6)) and the UC displacement $\mathbf{U}_{UC}$ is recovered using the compatibility condition of the Eq.(5).

In the absence of the external force $\mathbf{F}_{UC}$, the free vibration UC waves are obtained by solving the EVP of the Eq.(7) with at least one of $\{\omega, \lambda_x, \lambda_y\}$ as the unknown, which will be detailed in Section 3.4. Otherwise,

the forced vibration UC waves are solved by inverting the stiffness matrix of $\mathbf{\Lambda}_L\mathbf{D}_{UC}\mathbf{\Lambda}_R$ for the external force $\mathbf{\Lambda}_L\mathbf{F}_{UC}$ with the given values of $\{\omega, \lambda_x, \lambda_y\}$ as will be illustrated in Section 3.5.

To obtain the global free vibration wave $\mathbf{\Phi}_\alpha$ on the entire structure, the multiplication of the UC wave $\mathbf{U}_{UC}$ with the Floquet propagator $\lambda_x^{n_x}\lambda_y^{n_y}$ is performed as shown in Fig.4:

$$\mathbf{\Phi}_\alpha(n_x, n_y) = \lambda_x^{n_x}\lambda_y^{n_y}\mathbf{U}_{UC}, \tag{8}$$

where N_x, N_y are the number of UCs in the finite plate along x and y directions, while (n_x, n_y) is the coordinate of the UC on the grid ranging from $0, 1...N_x - 1$ and $0, 1...N_y - 1$ respectively and $\mathbf{\Phi}_\alpha(n_x, n_y)$ is the global free vibration wave $\mathbf{\Phi}_\alpha$ on the corresponding UC.

3.4 Numerical free vibration waves

The free vibration waves are the waves that propagate or decay in periodic structures without external force. As derived in the previous section, the free vibration waves are calculated on a single UC by solving the EVP (Eq.(7)) with external force absent. However, at a given frequency, there are still an infinite amount of free waves that satisfy the Eq.(7). A wave selection criterion following the rationale of the WBM is introduced (Tab.1).

Table 1: Sets of wave functions.

Set	Propagating constants and wave functions
1	Imposing $\lambda_x = \exp\left(\frac{2m\pi i}{N_x}\right), m = 0, 1...N_x - 1$ and solve for λ_y and UC waves $\mathbf{U}_{UC}$
2	Imposing $\lambda_y = \exp\left(\frac{2n\pi i}{N_y}\right), n = 0, 1...N_y - 1$ and solve for λ_x and UC waves $\mathbf{U}_{UC}$

where N_x, N_y are the number of UCs in the finite plate along x and y directions as well as λ_x and λ_y are the propagation constants.

If the obtained eigenvalue of λ_x or λ_y is of unit modulus, then the Floquet propagator only changes its phase through the UC grid and UC waves propagates through the entire struture. On the other hand, if the modulus of the eigenvalue is larger or smaller than 1, then an evanescent wave is obtained since it only propagates along one direction and decays along the perpendicular direction. In the numerical sense, the propagating waves and slowly evanescent waves build the dominant basis of the displacement field of the finite structure and the highly evanescent waves can be neglected in an approximation. Therefore, a dimensionless parameter $d = log(|\lambda_s|)$ $(s = x, y)$ that measures the magnitude of the decay is introduced and the waves are arranged in ascending order of d. The truncation criterion for the wave selection is proposed as $\mathrm{C} < \mathrm{C_T}$ to include the dominant wave basis, where only the first C percentage of waves are included and $\mathrm{C_T}$ is the given parameter for the truncation.

By expanding the EVP (Eq.(7)) with respect to λ_y, the quadratic form of the EVP is obtained as [3]:

$$(\mathbf{H}_0 + \lambda_y\mathbf{H}_1 + \lambda_y^2\mathbf{H}_2)\mathbf{U}_{UC}^{red} = 0 \tag{9}$$

where $\mathbf{H}_0$, $\mathbf{H}_1$ and $\mathbf{H}_2$ are the constant matrices associated with eigenvalue terms λ_y of different order.

Additionally, since the eigenvalue problem (Eq.(9)) is generally ill conditioned [17] due to the existence of highly evanescent waves resulting in extremely large and small eigenvalues, extra effort needs to be taken when solving the equation. In this work, the Cayley transform [18] is applied to avoid directly calculating extreme eigenvalues in the EVP solver. First, the Eq.(9) is linearized as follows:

$$\begin{bmatrix} \mathbf{0} & \beta\mathbf{I} \\ \mathbf{H}_0 & \mathbf{H}_1 \end{bmatrix} \begin{bmatrix} \mathbf{U}_{UC}^{red} \\ \lambda_y\mathbf{U}_{UC}^{red} \end{bmatrix} = \lambda_y \begin{bmatrix} \beta\mathbf{I} & \mathbf{0} \\ \mathbf{0} & -\mathbf{H}_2 \end{bmatrix} \begin{bmatrix} \mathbf{U}_{UC}^{red} \\ \lambda_y\mathbf{U}_{UC}^{red} \end{bmatrix} \tag{10}$$

where β is a scalar which is chosen to be the norm of $\mathbf{H}_1$ to avoid the ill conditioning due to the different order of magnitude between matrices.

Next, the Cayley tranform is applied to Eq.(10):

$$\begin{bmatrix} b\beta\mathbf{I} & \beta\mathbf{I} \\ \mathbf{H}_0 & \mathbf{H}_1 - b\mathbf{H}_2 \end{bmatrix} \begin{bmatrix} \mathbf{U}_{UC}^{red} \\ \lambda_y \mathbf{U}_{UC}^{red} \end{bmatrix} = \eta_y \begin{bmatrix} -c\beta\mathbf{I} & \beta\mathbf{I} \\ \mathbf{H}_0 & \mathbf{H}_1 + c\mathbf{H}_2 \end{bmatrix} \begin{bmatrix} \mathbf{U}_{UC}^{red} \\ \lambda_y \mathbf{U}_{UC}^{red} \end{bmatrix} \tag{11}$$

where the transformed eigenvalue $\eta_y = (\lambda_y + b)/(\lambda_y - c)$, as well as b and c are the constants imposed in this transformation.

Using the Cayley transform, the extremely large eigenvalues of λ_y are approaching 1 and small eigen values are approaching $-b/c$ in the transformed space. However, the original eigenvalues near the imposed constant c now become very large, which should be taken care of beforehand by chosing the transformation constants. To find a suitable value of the constant c, several random numbers are generated in a given domain and the constant correponding to the best condition number of the matrix $\mathbf{H}_0 + \lambda_y \mathbf{H}_1 + \lambda_y^2 \mathbf{H}_2$ is chosen as c. After solving the transformed EVP (Eq.(11)), the original eigenvalue λ_y is obtained by the back transformation $\lambda_y = (c\eta_s + b)/(\eta_y - 1 + \epsilon)$, where the constant ϵ is chosen above machine precision.

When the vector of master DOFs of the UC $\mathbf{U}_{UC}^{red}$ is solved, the UC waves are obtained as:

$$\mathbf{U}_{UC} = \mathbf{\Lambda}_R \mathbf{U}_{UC}^{red}. \tag{12}$$

The same procedure also applies when solving for the free vibration waves of the Set 2. With the UC waves obtained, the global free vibration waves $\mathbf{\Phi}_\alpha$ for the finite plate are obtained by expanding these UC waves $\mathbf{U}_{UC}$ through multiplication with the propagation constants λ_x and λ_y using Eq.8.

3.5 Numerical forced vibration waves

In this section, the procedure to calculate forced vibration waves using the WFEM is illustrated. First, periodic repetition of the finite plate and the given external force $\mathbf{F}$ is assumed as shown in Fig.6.

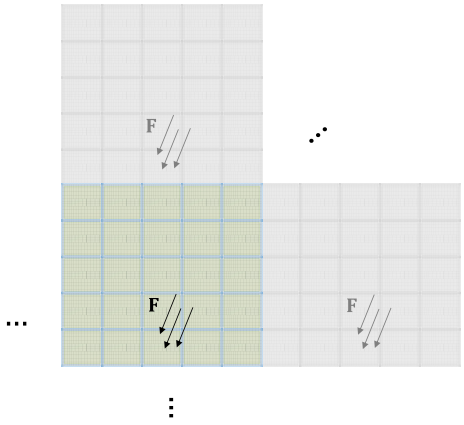

Figure 6: Assumption of infinite periodic repetition of the finite plate.

Next, the discrete Fourier transform (DFT) is applied to the external force $\mathbf{F}$ with respect to the UC grid, so that $\mathbf{F}$ is decomposed as UC modal forces $\mathbf{F}_{UC,mn}$:

$$\mathbf{F}_{UC}(m,n) = \frac{1}{N_x N_y} \sum_{n_x=0}^{N_x-1} \sum_{n_y=0}^{N_y-1} \lambda_{x,m}^{-n_x} \lambda_{y,n}^{-n_y} \mathbf{F}_{UC}(n_x, n_y) \tag{13}$$

where the propagation constants $\lambda_{x,m} = \exp(2\pi i m/N_x)$, $\lambda_{y,n} = \exp(2\pi i n/N_y)$. N_x, N_y are the number of UCs in the finite plate along x and y directions, while (n_x, n_y) is the coordinate of the each UC on the

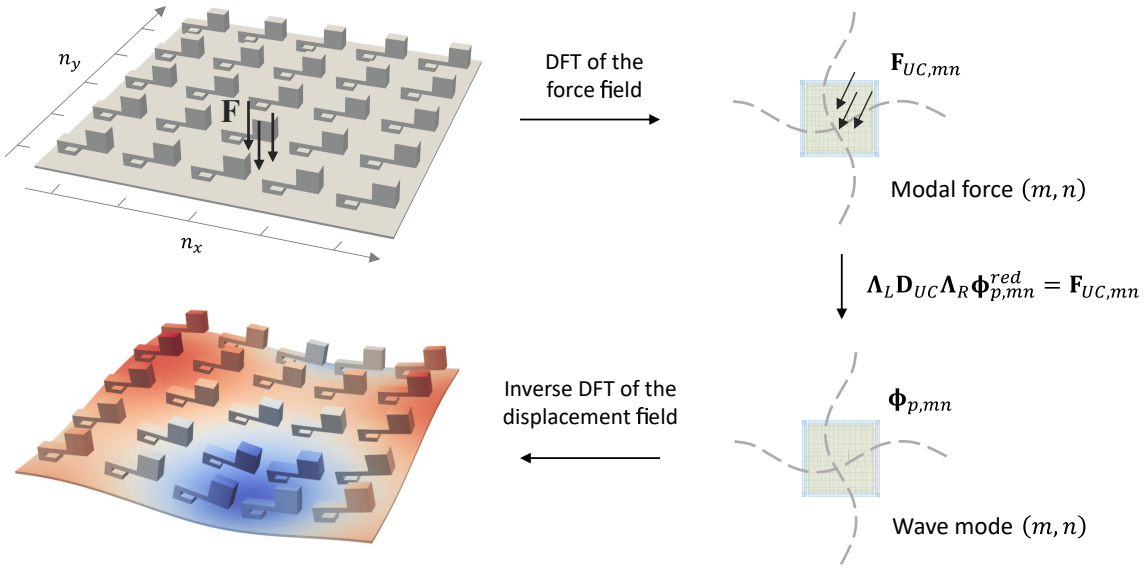

Figure 7: Calculation of the forced vibration wave.

grid ranging from $0, 1 \ldots N_x - 1$ and $0, 1 \ldots N_y - 1$ respectively. As a result of the DFT, the reciprocal coordinates m and n also range from $0, 1 \ldots N_x - 1$ and $0, 1 \ldots N_y - 1$. $\mathbf{F}_{UC}(n_x, n_y)$ is the given external force $\mathbf{F}$ on the UC at spatial coordinates (n_x, n_y) and $\mathbf{F}_{UC,mn}$ is the UC modal force corresponding to the projection of $\mathbf{F}$ on the discrete Fourier wave basis $\lambda_{x,m}^{n_x}\lambda_{y,n}^{n_y}$.

By expanding each UC modal force $\mathbf{F}_{UC}(m,n)$ to the entire finite plate through the multiplication with the corresponding discrete Fourier wave basis, the original external force $\mathbf{F}$ is recovered in the following summation:

$$\mathbf{F}_{UC}(n_x, n_y) = \sum_{m=0}^{N_x-1}\sum_{n=0}^{N_y-1} \lambda_{x,m}^{n_x}\lambda_{y,n}^{n_y}\mathbf{F}_{UC}(m,n)\,. \tag{14}$$

Therefore, the forced response vibration wave with respect to the external force $\mathbf{F}$ can be obtained through the summation of the forced vibration waves to each of the force component of $\lambda_{x,m}^{n_x}\lambda_{y,n}^{n_y}\mathbf{F}_{UC}(m,n)$. As each force component only changes its phase through the UC grid by multiplying the propagation constants of $\lambda_{x,m}$ and $\lambda_{y,n}$, the resulting forced vibration waves are solved on a single cell by applying the BF BCs (Fig.8).

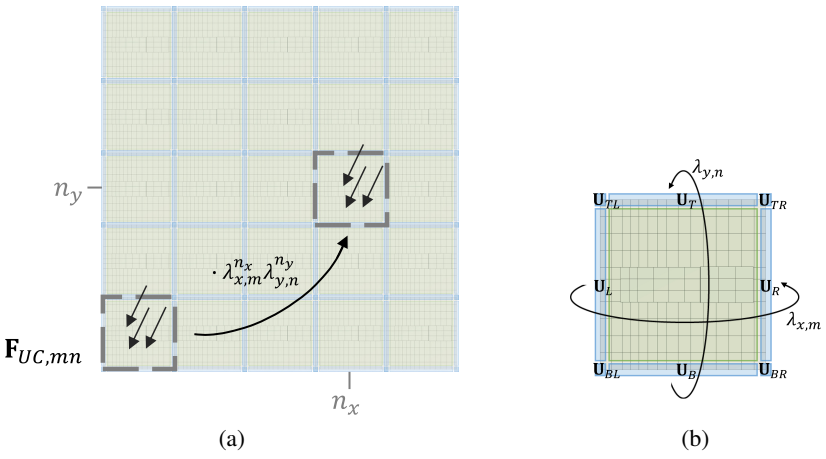

Figure 8: Periodicity of the force component (a) BF BCs of the UC in the reciprocal space (b).

Using the decomposition the Eq.14, the forced vibration waves with respect to each of modal force are

obtained by solving the following equation:

$$\mathbf{\Lambda}_L(\mathbf{D}_{UC}\mathbf{\Lambda}_R\mathbf{U}_{UC}^{red}(m,n)-\mathbf{F}_{UC}(m,n))=\mathbf{0}. \tag{15}$$

With the vector of $\mathbf{U}_{UC}^{red}(m,n)$ solved, the UC waves are obtained by re-expanding over the UC as:

$$\mathbf{U}_{UC}(m,n)=\mathbf{\Lambda}_R\mathbf{U}_{UC}^{red}(m,n). \tag{16}$$

Finally, through the inverse DFT the global forced vibration wave $\mathbf{\Phi}_p$ is obtained as:

$$\mathbf{\Phi}_p(n_x,n_y)=\sum_{m=0}^{N_x-1}\sum_{n=0}^{N_y-1}\lambda_{x,m}^{n_x}\lambda_{y,n}^{n_y}\mathbf{U}_{UC}(m,n) \tag{17}$$

where $\mathbf{\Phi}_p(n_x,n_y)$ is the global wave $\mathbf{\Phi}_p$ on the UC located at (n_x,n_y).

3.6 Solving the system

With the free and forced vibration waves obtained, the approximated displacement field is represented by the linear superposition with unknown contribution factors as defined in the Eq.(18).

$$\hat{\mathbf{u}}=\sum_{\alpha=1}^{N}\mathrm{c}_\alpha\mathbf{\Phi}_\alpha+\mathbf{\Phi}_p. \tag{18}$$

Next, the boundary conditions are imposed in a collocation sense at all FE nodes along the boundary [19]:

$$\mathcal{B}(\hat{\mathbf{u}})=0 \tag{19}$$

where $\mathcal{B}$ measures the mismatch of the boundary conditions using the approximated displacement field. Therefore, a linear system equation is obtained and the contribution factors c_α are solved for:

$$\mathbf{G}\mathbf{c}=\mathbf{b}, \tag{20}$$

where $\mathbf{G}$ is a dense matrix corresponding to the free vibration waves at the FE nodes along the boundary, the vector $\mathbf{b}$ corresponds to the forced vibration wave at the FE nodes along the boundary and the imposed constraints of the displacement, the vector $\mathbf{c}$ is the vector of contribution factors c_α.

Finally, the displacement field at the given frequency is obtained by imposing the contribution factors back to the Eq.(18). After that, the process is performed again for the next frequency of interest.

4 Numerical results

In this section, the strengths of the WBM in terms of computation time for forced response analysis of flat rectangular periodic plates are demonstrated by presenting a time assessment of the WBM as compared to the UC substructuring method [13] for the differently sized plates. Before doing so, a convergence study of the GBMS inputs as well as the truncation factor of WBM is first performed for a clamped finite plate composed of 5×5 UCs to find the proper input parameters.

4.1 UC modal reduction

Following the design in [20], a UC consisting of a $30\times30\times1$ mm^3 aluminum plate with a beam-shaped PMMA resonator on the top is considered. The geometric parameters and material properties for the host

structure and resonator follow the data provided in the corresponding paper. The UC is discretized using 114 quadratic hexahedral solid elements, which leads to 4557 DOFs of the UC FE model in total (Fig.3(a)).

To find the proper input parameters of the GBMS, the computation of the eigenfrequencies of a clamped finite plate composed of 5×5 GBMS reduced UCs is assessed for different numbers of interior modes and interface modes. The relative errors on these eigenfrequencies are computed against the corresponding finite plate FOM. At first, the interface DOFs are kept and only the interior modal reduction is performed (Fig.9). It is shown that from $n_{\mathrm{I}} = 30$ interior modes onwards, the improvement of the accuracy is limited. Considering 30 interior modes, the interface reduction is now also performed (Fig.10), revealing that the highest relative error stagnates from $n_{\mathrm{A}} = 50$ interface modes. Therefore, 30 interior modes and 50 interface modes are chosen to be suitable inputs of the GBMS procedure.

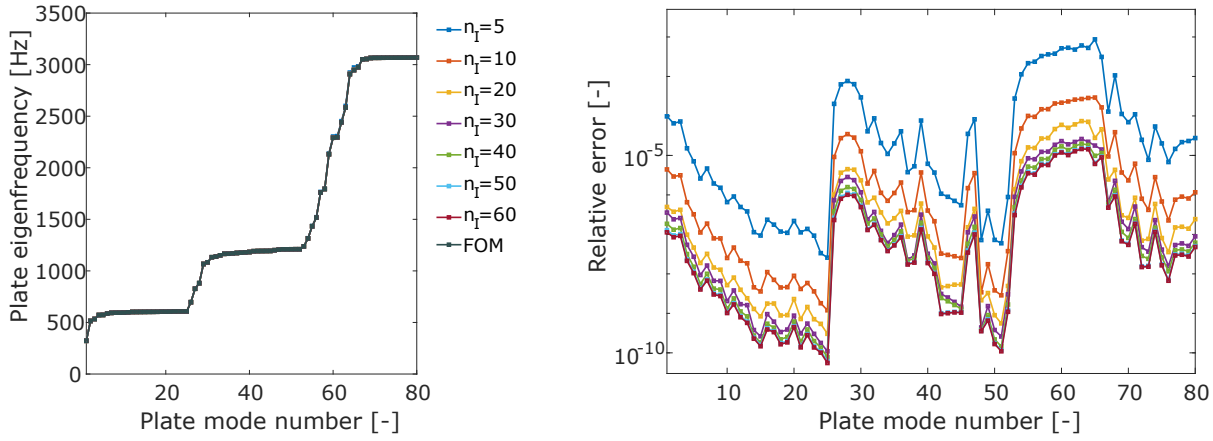

(a) (b)

Figure 9: Eigenfrequencies (a) and relative error of the eigenfrequencies (b) computed for the clamped finite plate assembly of 5×5 BMS UC ROMs, considering different number of interior modes.

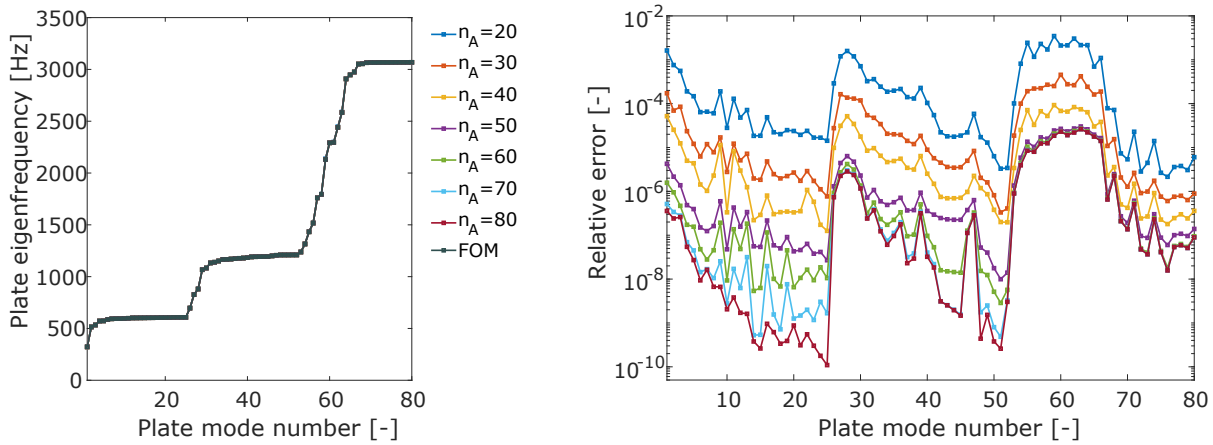

(a) (b)

Figure 10: Eigenfrequencies (a) and relative error of the eigenfrequencies (b) computed for the clamped finite plate assembly of 5×5 GBMS UC ROMs, considering different interface modes.

4.2 Selection of the truncation factor

With the reduced UC model obtained, the WBM and the UC substructuring method is applied to the clamped finite plate composed of 5×5 UC ROMs (Fig.11) to calculate the point-to-point FRF over the frequency values of 0:2:1000 Hz. As the WBM relies on the GBMS reduced UC model, the accuracy of the WBM will not exceed that of the UC substructuring method. Therefore, the corresponding GBMS UC substructuring solution serves as the reference. In the following cases, the truncation factor $\mathrm{C_T}$ increases from 40 to 100. For each truncation factor, the FRF and the relative error are shown in Fig.12. The accuracy of the WBM increases as the truncation factor grows (Fig.12(b)). Even though the error for $\mathrm{C_T} = 60$ is now acceptable, the truncation factor can be further increased to reduce this error, with $\mathrm{C_T} = 100$ resulting in the relative error around 10^{-8} between the WBM and the UC substructuring solutions. Therefore, $\mathrm{C_T} = 100$ is chosen as the truncation factor in the following time assessment.

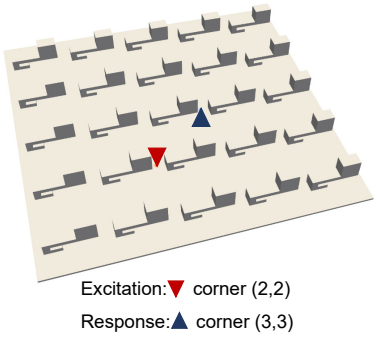

Figure 11: The finite metamaterial structures composed of 5×5 UCs. The plate is excited by a single unit normal point force.

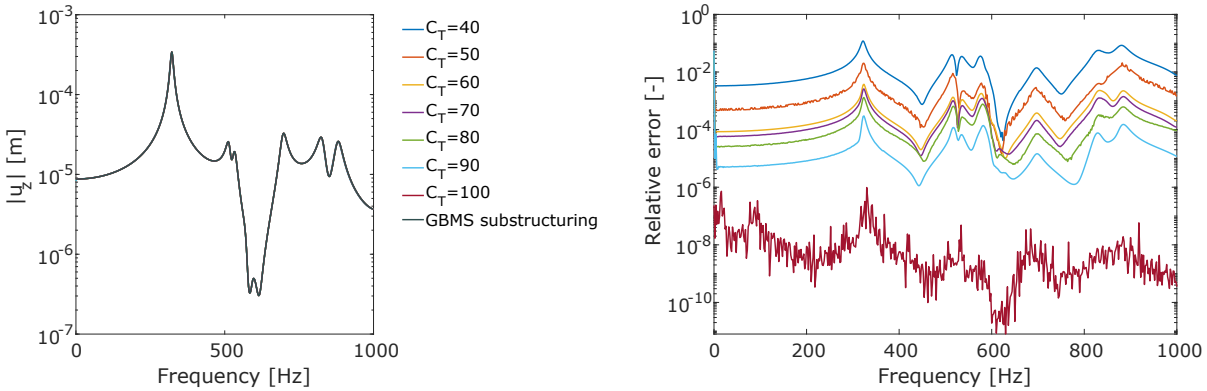

(a) (b)

Figure 12: FRF (a), relative errors over the frequency (b) computed for the clamped finite plate assembly of 5×5 UC ROMs considering different truncation factors.

4.3 Overview of the study cases

In order to perform the time assessment, the point-to-point FRF in the frequency range 0:2:1000 Hz is calculated for four cases using the WBM and the UC substructuring method: finite metamaterial structures composed of 5×5, 10×10, 20×20, 30×30 UCs as shown in Fig.13. The FOM solution is solved in the frequency range 0:50:1000 Hz, which serves as the reference to verify the accuracy of both approaches. For the WBM and the UC substructuring method, the UC FE model is composed of 114 quadratic hexahedral

elements and reduced with 30 interior modes and 50 interface modes. For the WBM, the truncation factor C_T is set as 100 to include all of the wave functions.

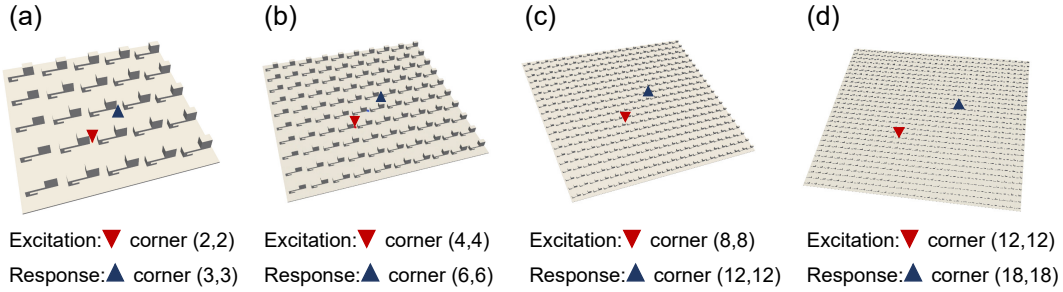

Figure 13: The finite metamaterial structures composed of 5×5, 10×10, 20×20, 30×30 UCs. The plates are all excited by a single unit normal point force.

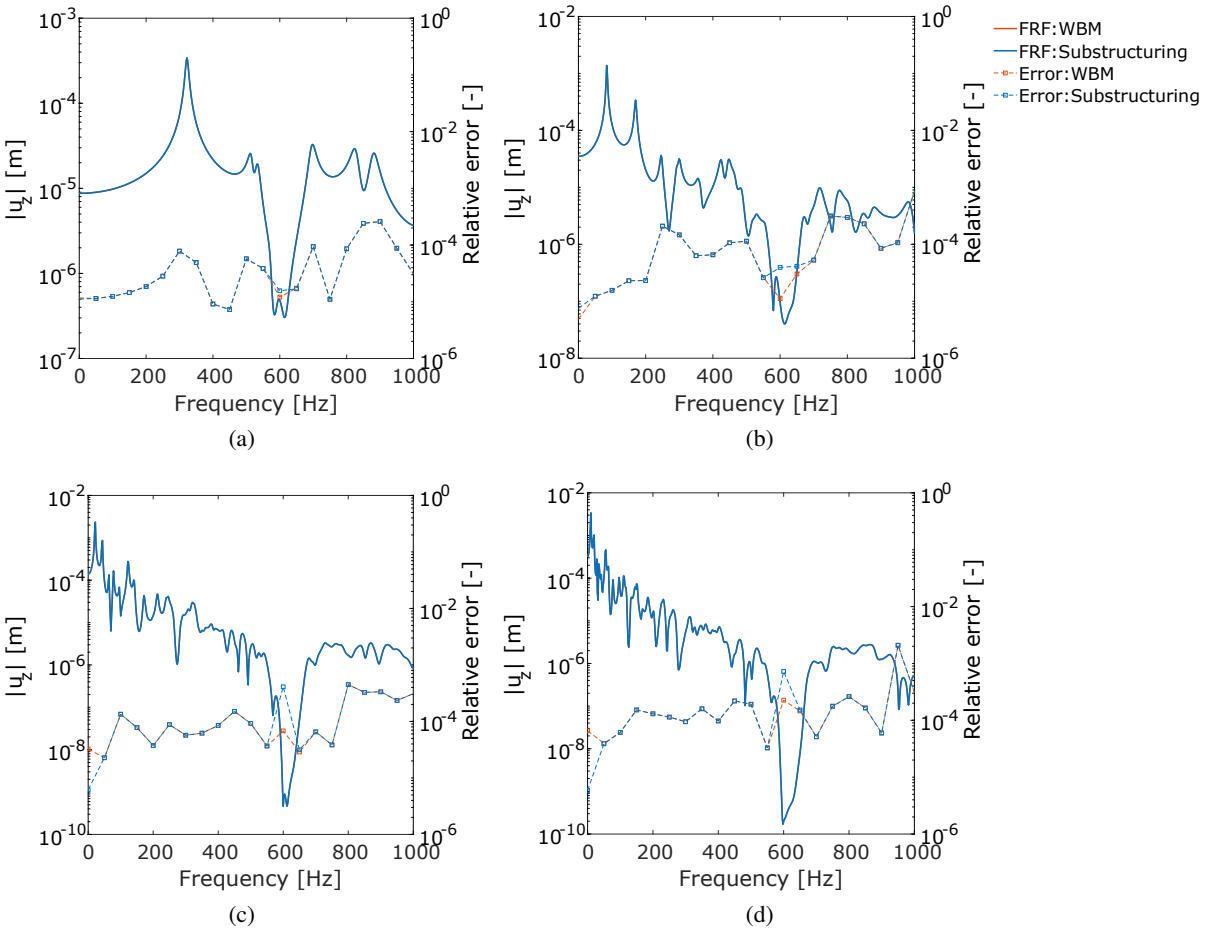

Figure 14: FRF calculations and relative error for each reduced model of finite structures of 5×5 (a), 10×10 (b), 20×20 (c), 30×30 (d) UCs.

In Fig.14, the accuracy and the computation time of the FRF calculations using the WBM and the UC substructuring method are shown for the considered cases. Following [13], the assembled matrix using the substructuring method is reduced with a global modal reduction using respectively 200, 1000, 5000 and 12000 global normal modes for the increasing plate sizes as well as a static enrichment vector for the applied point force during the offline calculation and finally the FRF can be efficiently solved on the reduced

matrix for any arbitary frequency resolution as the online phase. The FRF curves for all cases clearly show the stop band between 597 Hz and 656 Hz which leads to strong vibration attenuation as expected for this metamaterial design [21]. The error over the frequency range on the right hand side indicates that the WBM achieves the same accuracy as the UC substructuring method. In particular, the WBM performs better around the stop band than the other method, as the truncated global eigen-modes used in the substructuring approach has difficulty to efficiently approximate the forced response at the superposed anti-resonance of a large number of UCs.

4.4 Time assessment

A summary of the model size and the computation time needed are given in the Tab.2 and the Tab.3. With increasing plate size, the resulting reduced model dimensions become smaller using the WBM as compared to the UC substructuring method. Computation time is obtained using an Intel Xeon Gold 6140 Processor with 192 GB RAM and 18 cores. The scaling property of both methods is estimated using the asymptotic computational complexity. By assuming that the computation time T is a polynomial function of the number of the FOM DOFs N, then the leading term dominates as N grows large enough: $T \sim O(N^p)$. The index p is approximated through a linear fit between $log(T)$ and $log(N)$. Using the computation time recorded in the Tab. 3, the scaling index p for the WBM and the UC substructuring method is estimated as 1.38 and 2.17, respectively. Whereas for smaller plate assemblies the UC substructuring method outperforms the WBM in terms of model size and computational time, the WBM scales more favorably and outperforms the UC substructuring method for larger finite plate assemblies.

Table 2: Model sizes of the WBM and the UC substructuring method.

Model	WBM	UC substructuring method
5×5 UCs	2060	201
10×10 UCs	4120	1001
20×20 UCs	8240	5001
30×30 UCs	12360	12001

Table 3: Computation time of the WBM and the UC substructuring method.

Model	WBM	UC substructuring method
5×5 UCs	124.4 s	21.7 s
10×10 UCs	2229.0 s	371.3 s
20×20 UCs	9270.9 s	8318.7 s
30×30 UCs	19121.8 s	53315.6 s

5 Conclusion

In this paper, the WBM was investigated and applied to build efficient ROMs for two dimensional periodic structures by taking full advantage of the periodicity. This approach approximates the solution using a linear superposition of the waves, which can be cheaply calculated on a single UC, while conventional model reduction approaches need to directly deal with the assembled matrix of the global structure. Compared with the UC substructuring method, this approach achieves similar accuracy and shows a favorable scaling in both computation time and model size for the assembly of large numbers of UCs due to a favorable growth rate. Although the growth rate of the computational effort of the WBM is lower, it should be pointed out that the ROM of the WBM is built at every frequency value of interest. Therefore, it is expected that the computation time of the WBM grows linearly with an increasing frequency resolution, while that of the UC substructuring method is independent of the frequency resolution as the ROM is built once for all frequency values. To overcome this problem, a fast frequency sweep technique will be incorporated in future work.

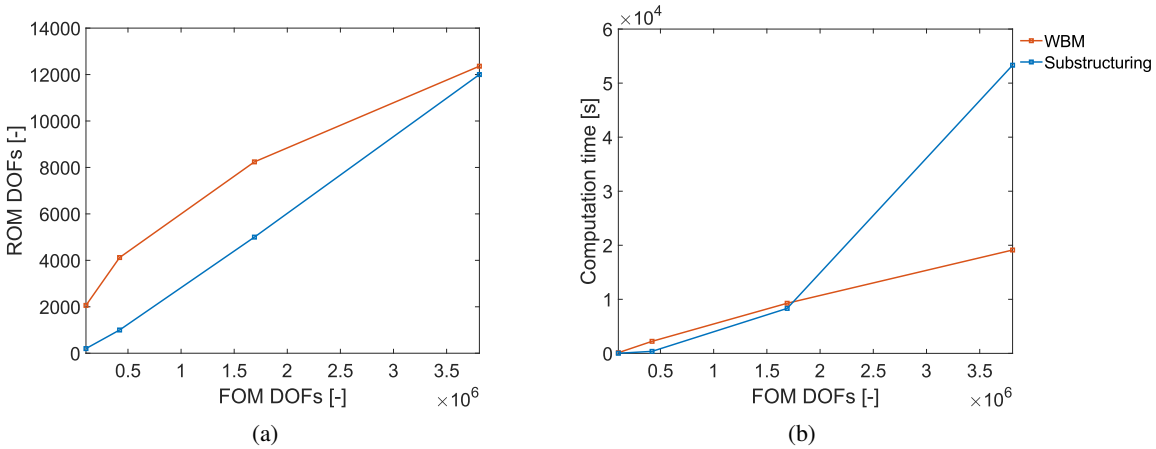

Figure 15: Model size (a) and computation time (b) of the WBM and the UC substructuring method for growing FOM sizes.

Acknowledgements

The work has been funded by the project "MOR4MDesign", which is part of the MacroModelMat (M3) research program coordinated by Siemens (Siemens Digital Industries Software, Belgium) and funded by SIM (Strategic Initiative Materials in Flanders) and VLAIO (Flanders Innovation & Entrepreneurship Agency). The Research Fund KU Leuven is also gratefully acknowledged for its support. The research of L. Van Belle (fellowship no. 1271621N) is funded by a grant from the Research Foundation – Flanders (FWO).

References

[1] Z. Liu, X. Zhang, Y. Mao, Y. Zhu, Z. Yang, C. T. Chan, and P. Sheng, "Locally resonant sonic materials," *science*, vol. 289, no. 5485, pp. 1734–1736, 2000.

[2] J. Li and C. T. Chan, "Double-negative acoustic metamaterial," *Physical Review E*, vol. 70, no. 5, p. 055602, 2004.

[3] B. R. Mace and E. Manconi, "Modelling wave propagation in two-dimensional structures using finite element analysis," *Journal of Sound and Vibration*, vol. 318, no. 4-5, pp. 884–902, 2008.

[4] D. Mead, "A general theory of harmonic wave propagation in linear periodic systems with multiple coupling," *Journal of Sound and Vibration*, vol. 27, no. 2, pp. 235–260, 1973.

[5] M. Collet, M. Ouisse, M. Ruzzene, and M. Ichchou, "Floquet–bloch decomposition for the computation of dispersion of two-dimensional periodic, damped mechanical systems," *International Journal of Solids and Structures*, vol. 48, no. 20, pp. 2837–2848, 2011.

[6] D. Krattiger and M. I. Hussein, "Bloch mode synthesis: Ultrafast methodology for elastic band-structure calculations," *Physical Review E*, vol. 90, no. 6, p. 063306, 2014.

[7] D. Krattiger and M. I. Hussein, "Generalized bloch mode synthesis for accelerated calculation of elastic band structures," *Journal of Computational Physics*, vol. 357, pp. 183–205, 2018.

[8] M. I. Hussein, "Reduced bloch mode expansion for periodic media band structure calculations," *Proceedings of the Royal Society A: Mathematical, Physical and Engineering Sciences*, vol. 465, no. 2109, pp. 2825–2848, 2009.

[9] L. Sangiuliano, C. Claeys, E. Deckers, and W. Desmet, "Influence of boundary conditions on the stop band effect in finite locally resonant metamaterial beams," *Journal of Sound and Vibration*, vol. 473, p. 115225, 2020.

[10] J.-M. Mencik and D. Duhamel, "Dynamic analysis of periodic structures and metamaterials via wave approaches and finite element procedures," in *8th International Conference on Computational Methods in Structural Dynamics and Earthquake Engineering*, 2021.

[11] S. van Ophem, E. Deckers, and W. Desmet, "Efficient assembly of unit cells with krylov based model order reduction," in *PROCEEDINGS OF INTERNATIONAL CONFERENCE ON NOISE AND VIBRATION ENGINEERING (ISMA2018)/INTERNATIONAL CONFERENCE ON UNCERTAINTY IN STRUCTURAL DYNAMICS (USD2018)*. KATHOLIEKE UNIV LEUVEN, DEPT WERKTUIGKUNDE, 2018, pp. 445–456.

[12] J.-M. Mencik, "Model reduction based on matrix interpolation and distorted finite element meshes for dynamic analysis of 2d nearly periodic structures," *Finite Elements in Analysis and Design*, vol. 188, p. 103518, 2021.

[13] L. Van Belle *et al.*, "Fast forced response calculations of finite metamaterial plates using a generalized bloch mode synthesis based sub-structuring approach," in *Proceedings of Euronoise*, 2021.

[14] C. Droz, R. Boukadia, and W. Desmet, "A multi-scale model order reduction scheme for transient modelling of periodic structures," *Journal of Sound and Vibration*, p. 116312, 2021.

[15] R. F. Boukadia, C. Droz, M. N. Ichchou, and W. Desmet, "A bloch wave reduction scheme for ultrafast band diagram and dynamic response computation in periodic structures," *Finite Elements in Analysis and Design*, vol. 148, pp. 1–12, 2018.

[16] E. Deckers, O. Atak, L. Coox, R. D'Amico, H. Devriendt, S. Jonckheere, K. Koo, B. Pluymers, D. Vandepitte, and W. Desmet, "The wave based method: An overview of 15 years of research," *Wave Motion*, vol. 51, no. 4, pp. 550–565, 2014.

[17] Y. Waki, B. Mace, and M. Brennan, "Numerical issues concerning the wave and finite element method for free and forced vibrations of waveguides," *Journal of Sound and Vibration*, vol. 327, no. 1-2, pp. 92–108, 2009.

[18] C. Schröder, "Palindromic and even eigenvalue problems-analysis and numerical methods," 2008.

[19] D. Huybrechs and A.-E. Olteanu, "An oversampled collocation approach of the wave based method for helmholtz problems," *Wave Motion*, vol. 87, pp. 92–105, 2019.

[20] L. Van Belle, C. Claeys, E. Deckers, and W. Desmet, "On the impact of damping on the dispersion curves of a locally resonant metamaterial: Modelling and experimental validation," *Journal of Sound and Vibration*, vol. 409, pp. 1–23, 2017.

[21] L. Van Belle *et al.*, "Fast metamaterial design optimization using reduced order unit cell modeling," *Proceedings of ISMA 2020*, 2020.